Journal of Magnetism and Magnetic Materials 321 (2009) 2232–2238

Contents lists available at ScienceDirect

Journal of Magnetism and Magnetic Materials

journal homepage: www.elsevier.com/locate/jmmm

Fe monolayers on InAs(0 0 1): An *in situ* study of surface, interface and volume magnetic anisotropy

F.M. Römer [a,*], C. Hassel [a], Kh. Zakeri [b], C. Tomaz [a], I. Barsukov [a], R. Meckenstock [a], J. Lindner [a], M. Farle [a]

[a] Fachbereich Physik and Center for Nanointegration (CeNIDE), Universität Duisburg-Essen, Lotharstr. 1, 47048 Duisburg, Germany
[b] Max-Planck Institute of Microstructure Physics, Weinberg 2, D-06120 Halle, Germany

ARTICLE INFO

Article history:
Received 25 September 2008
Available online 11 February 2009

PACS:
75.30.Gw
75.70.Ak
76.50.+g

Keywords:
Magnetic anisotropy
Magnetic thin film
Ferromagnetic resonance

ABSTRACT

The magnetic anisotropy of epitaxial Fe films with thicknesses in the range of 2−142 monolayers (ML) grown on {4 × 2} reconstructed InAs(0 0 1) was investigated by *in situ* ferromagnetic resonance. The easy magnetization direction was found to be parallel to the [1 $\bar{1}$ 0]-direction for Fe films below 4 ML, while it rotates by 45° toward the [1 0 0]-direction. It is observed that both surface-interface and volume contribution to the perpendicular anisotropy favor an easy axis perpendicular to the film plane. The cubic surface-interface anisotropy is relatively large with easy axes along ⟨1 $\bar{1}$ 0⟩-directions in contrast to the volume contribution which favors easy axes along the ⟨1 1 0⟩-directions. The volume contribution is found to be larger than the Fe bulk cubic anisotropy. A thickness independent uniaxial anisotropy has been found in films with a thickness of 2 up to 142 ML.

1. Introduction

Besides the system Fe/GaAs a second promising candidate for '*spintronics*' applications is the Fe/InAs(1 0 0) system. InAs has a narrow band-gap (less than 0.4 eV) and, therefore, the Fe/InAs interface forms an ideal ohmic contact as reported by Xu et al. [1]. Moreover, InAs is a very good candidate for high speed electronics and infrared optoelectronics, due to its large electron mobility (larger than 3.2 $m^2/(V\,s)^{-1}$) [2] and considerably high Rashba effect [3].

The epitaxial growth of Fe on {4 × 2} reconstructed InAs(0 0 1) was reported within the last few years by several groups [1,4–9]. It is shown that arsenic and indium react partially with the Fe layer at the interface and a segregation of the species (mainly In) on the surface was observed [6,7]. It was demonstrated by Teodorescu et al. that the Fe/InAs interface is much less reactive than the one of Fe/GaAs and the interface formation was found to be restricted to only 1 ML at the interface [10–12].

The spin injection through an InAs interface was predicted by Zwierzycki et al. [13] and later demonstrated by Ohno et al. [14] who found a circular polarization of about −12% at $T = 6.5$ K under an applied magnetic field of 10 T. The interface perfection is the key for magneto-electronic applications, where a spin-polarized current is to be injected into the semiconductor. The phase diagram of the InAs(0 0 1) surface structure studied by Yamaguchi and Horikoshi [15] using high-energy electron diffraction (RHEED), scanning tunneling microscopy (STM) and Monte Carlo simulations shows a phase transition between an As-stabilized {2 × 4}and an In-stabilized {4 × 2} surface reconstruction. Since according to their studies the {4 × 2} surface reconstruction is more In-rich in order to avoid possible formation of FeAs alloys (magnetically 'dead' layers) the {4 × 2} surface reconstruction was chosen for our investigation.

In this paper the epitaxial growth and the magnetic anisotropy of Fe monolayers (ML) grown on {4 × 2} InAs are reported. All structural and magnetic characterizations were performed *in situ* under ultrahigh vacuum (UHV) conditions at a microwave frequency of 9.3 GHz, while supporting frequency dependent investigations as well as the measurements on Ag/Au capped films were conducted *ex situ*.

2. Experimental details

The 4 × 4 mm^2 pieces cut from commercially available n-type InAs(0 0 1) wafers has been used as substrates. Before inserting it into UHV, it was cleaned in an ultrasonic bath using pure acetone and isopropanol and then immediately transferred into the UHV chamber. Inside the UHV chamber the substrates were firstly outgassed by slightly rising the temperature to about 760 K. In order to reach the wished {4 × 2} surface reconstruction, the substrate was sputtered and subsequently annealed several times. The annealing temperature was about 760 K while the Ar^+-ions used

* Corresponding author. Tel.: +49 2033794411.
E-mail address: florian.roemer@uni-due.de (F.M. Römer).

0304-8853/$ - see front matter © 2009 Elsevier B.V. All rights reserved.
doi:10.1016/j.jmmm.2009.01.047

for the sputter process had an energy of 0.5 keV with a partial Ar^+ pressure of about 2×10^{-5} mbar and an Ar^+ current density of about 3–5 μA/cm^2. This cleaning process is similar to the one used in Ref. [9]. The cleanliness of the substrates was revealed by Auger electron spectroscopy (AES). Although the intensity of the indium MNN transition with respect to the arsenic LMM transition already is expected to be very large due to the different kinds of transitions, a comparison of our AES measurements with the spectra taken from the *pure* elements [17] shows that it is even larger than the expectation for the case that equal amounts of the two elements are exposed to the electron beam. This finding thus shows that the surface is In-rich. An AES spectrum and a typical low-energy electron diffraction (LEED) pattern of the clean {4 × 2} InAs surface is shown in the inset of Fig. 1(a), while Fig. 1(c) presents the schematic representations of possible {4 × 2} reconstructions taken from [15]. As all unit cells have the same symmetry they cannot be distinguished by LEED. While the common feature of all structures is that indium dimers form parallel to the [1 1 0]-direction in real space, the difference is the amount of indium terminating the surface. Since arsenic was found to desorb more easily from the surface than indium [15], the structures with more indium will be favored when using high temperatures during sample preparation.

At this point it should be noted that a confusing notation in literature is found concerning the terminology of the crystallographic directions in combination with the notation used for the surface reconstruction [6,9,18]. The notation {4 × 2} used by us specifies the orientation of the pattern, with the ×2-direction along [1 1 0] and the ×4-direction along [1 $\bar{1}$ 0]. This notation is consistent with that used to define the {4 × 2} and {2 × 4} reconstructions of GaAs(1 0 0) [15]. It is essential to know the orientation of the LEED pattern, since the ⟨1 1 0⟩- and ⟨1 $\bar{1}$ 0⟩-directions are inequivalent with respect to the bulk structure [16]. In the [1 0 0] direction, zincblende structure III–V semiconductors consist of alternating layers of anions (e.g. As) and cations (e.g. In). If the crystal is terminated by a layer of anions, their dangling bonds lie in the (1 1 0)-plane (i.e. are oriented along [1 $\bar{1}$ 0]). If the crystal is terminated by a layer of cations, their dangling bonds lie in the (1 $\bar{1}$ 0)-plane (i.e. are oriented along [1 1 0]). A schematic illustration of the anion's and cation's dangling bonds in (0 0 1) surfaces of III–V semiconductors with zincblende structure is given in Fig. 1(b). For the {4 × 2} pattern, the periodicity is doubled along the direction of the indium dangling bonds, and quadrupled along the direction of the arsenic dangling bonds (see also the structure models of Fig. 1(c)).

Upon inspection of the LEED pattern one observes sharp quarter order spots, while the half order spots are surrounded by streaks. This indicates that the periodicity along the [1 1 0]-direction in k-space ([1 $\bar{1}$ 0]-direction in real space) is less pronounced than along the [1 $\bar{1}$ 0]-direction in k-space ([1 1 0]-direction in real space). This streakiness must thus result from a reduction of the periodicity parallel to the ×2-direction in real space, which is the direction parallel to the indium dimer rows (see structure models in Fig. 1(c)). In Refs. [15,16] the streakiness was suggested to be the result of an occurrence of structural domains with {4 × 2} and c{8 × 2} reconstructions. A c{8 × 2} reconstructed unit cell results when neighboring {4 × 2} unit cells are shifted by half their length along the [1 $\bar{1}$ 0]-direction with respect to each other. A random distribution of the two reconstruction types would, in fact, leave the quarter order spots unaffected, while the half order ones become streaky. For a random distribution, however, one would expect the half order spots to be wiped out completely. From the fact that there are still half order spots visible in addition to the streaks we conclude that the areas with {4 × 2} reconstructions dominate the surface morphology.

The Fe films were grown at room temperature (RT) by molecular beam epitaxy with a deposition rate of 0.5 ML/min monitored by a quartz micro balance, which can measure thicknesses in the order of 0.01 nm. However all thicknesses are rounded to full ML. The basic pressure of the chamber wasabout 1×10^{-10} mbar rising during Fe-deposition up to about 7×10^{-10} mbar. A LEED and an AES analysis was performed to verify the film quality. It has been observed that the LEED pattern disappears immediately after the deposition of the first Fe layer and only a diffuse LEED pattern appears with broad spots around 19 ML. Such an observation is reported also by other groups [1,5]. As our magnetic analysis shows well defined magnetic symmetry for the Fe films, the diffuse LEED pattern could be the result of a floating Indium layer on top of the film or because of island-like growth, which enables the Auger electrons to leave the substrate between the islands even for larger Fe thicknesses. Indeed, our AES results show that the In-signal does not disappear even for Fe thicknesses of 19 ML (see Fig. 2), while it disappears for thicker Films.

In order to get an insight into the onset of long range ferromagnetic order ML of Fe were grown from 0.6 up to 3 ML. Ferromagnetic resonance (FMR) experiments were performed as a function of the nominal number of Fe layers at RT using a microwave frequency of 9.3 GHz. The external magnetic field was applied along the [1 $\bar{1}$ 0]-direction (easy axis, see below).

In order to determine the magnetic anisotropy *in situ* FMR measurements have been carried out immediately after growth. A full in-plane and out-of-plane angular dependence (using magnetic fields of up to 1.3 T) of the FMR signal was performed *in situ* at a microwave frequency of 9.3 GHz. This unique ability of our experimental setup allows a precise determination of the magnetic anisotropy constants.

A straightforward way to extract the anisotropy constants from the angular dependent data is provided the free energy approach

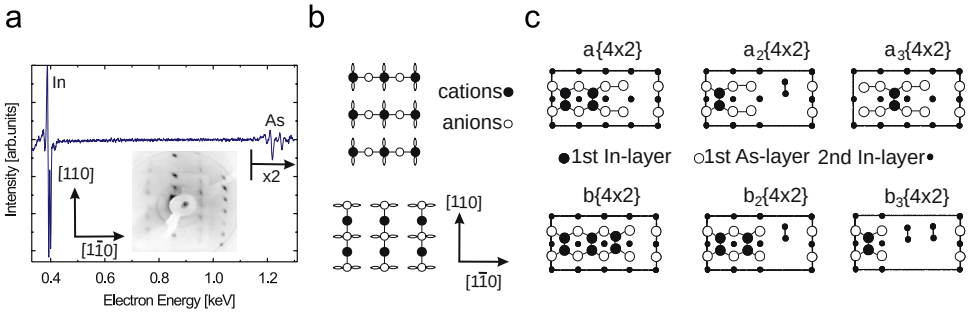

Fig. 1. (a) Typical AES spectrum of a clean InAs substrate. Inset shows a LEED-pattern taken at an electron energy of 56 eV showing a 4 × 2 reconstruction with well defined quarter order spots and streaky half order spots reciprocal k-vectors are shown. (b) Schematic representation of the direction of the dangling bonds for the (0 0 1)-plane of a III–V semiconductor surface [16]. Indium atoms are cations. (c) Schematic illustration of possible atomic structures for {4 × 2} InAs(0 0 1) (taken from Ref. [15]).

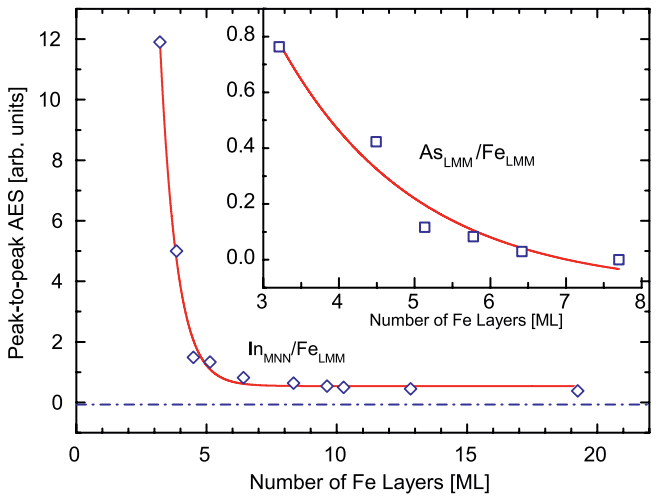

Fig. 2. Ratio of the AES peak-to-peak intensities of the Indium MNN transition to the Fe LMM one. The inset shows the AES peak-to-peak intensities of the arsenic LMM line with respect to the Fe LMM line. The solid curves are guides to the eye.

[19,20]. In FMR, the precession of the total magnetic moment with free energy, F, occurs at the resonance frequency given by

$$\left(\frac{\omega}{\gamma}\right)^2 = \frac{1}{M^2\sin^2(\theta)}\left[\frac{\partial^2 F}{\partial\theta^2}\frac{\partial^2 F}{\partial\phi^2} - \left(\frac{\partial^2 F}{\partial\theta\partial\phi}\right)^2\right] \quad (1)$$

The partial derivatives are evaluated at angles of θ and ϕ (polar and azimuthal angle of M) which minimize F and γ is the gyromagnetic ratio. Note that the resonance frequency is related to the second derivatives of F, and thus is essentially a measure of the *curvature* of F, or the stiffness of M. In the experiments described below the magnetization is perturbed at a constant microwave frequency ω_p and F is modified by varying an applied external field. The fields needed to change F such that $\omega = \omega_p$ is referred to as the resonance field, B_{res}.

For a ferromagnetic film with cubic symmetry and (0 0 1)-orientation the free energy density F includes the Zeeman energy, the demagnetizing energy, the perpendicular uniaxial $K_{2\perp}$ as well as the cubic K_4 anisotropy energy density. In the case of ultrathin ferromagnetic films on semiconducting substrates an in-plane anisotropy $K_{2\parallel}$ of uniaxial character has usually to be, yielding

$$\begin{aligned} F &= -\vec{M}\cdot\vec{B} + \left(\frac{\mu_0}{2}M^2 - K_{2\perp}\right)\alpha_z^2 + K_{2\parallel}\alpha_{\mathrm{e.a.}}^2 \\ &\quad + K_4(\alpha_x^2\alpha_y^2 + \alpha_x^2\alpha_z^2 + \alpha_y^2\alpha_z^2) \\ &= -MB[\sin\theta\sin\theta_B\cos(\phi-\phi_B) + \cos\theta\cos\theta_B] \\ &\quad + \left(\frac{\mu_0}{2}M^2 - K_{2\perp}\right)\cos^2\theta + K_{2\parallel}\sin^2\theta\cos^2(\phi-\delta) \\ &\quad + K_4\sin^2\theta - \frac{K_4}{8}(7+\cos 4\phi)\sin^4\theta \end{aligned} \quad (2)$$

Here $\theta_B(\phi_B)$ is the polar (azimuthal) angle of the external field B with respect to [0 0 1]([1 0 0]), $\theta(\phi)$ is the polar(azimuthal) angle of the magnetization with respect to the [0 0 1]([1 0 0])-direction and the α_i are the direction cosines defined by the coordinate system given by the cubic ⟨1 0 0⟩-axes. δ is the angle between the easy axis of the twofold in-plane anisotropy $K_{2\parallel}$ with respect to the easy axis of the fourfold anisotropy, $\alpha_{\mathrm{e.a.}}$ is the direction cosine with respect to the easy *in-plane* direction. Upon inserting the free energy derivatives into Eq. (1) one obtains explicit resonance equations linking resonance frequency and field within specific planes. A detailed description may be found e.g. in [21,22].

3. Results and discussion

3.1. The onset of the RT ferromagnetic order

In Fig. 3 the thickness dependence of the FMR resonance field B_{res} (a) and the FMR line width ΔB_{pp} (b) measured at RT are shown. The first ferromagnetic signal was observed for a film thickness of 1.6 ML with the lowest resonance field and largest FMR line width. The small value of B_{res} is due to the fact that for this thickness, the cubic anisotropy (it will be called $K_{4\parallel}$, as we will show below that the films are to some extend distorted) is $K_{4\parallel} \approx 0$. As we will show that the cubic anisotropy favors the ⟨1 0 0⟩-axes like in bulk Fe, the FMR along the cubic hard [1 $\bar{1}$ 0]-direction takes place at lower fields (i.e. at a more easy direction) in the absence of $K_{4\parallel}$. The large ΔB_{pp} can be attributed to the large size distribution of the 3D-like Fe clusters that form in the first stage of the growth. The coalescence of Fe clusters and formation of a continuous film take place around 5 ML as found by RHEED [18] and STM studies [9].

3.2. Magneto crystalline anisotropy constants

A typical polar (external field varied in a plane defined by the film normal and the [1 $\bar{1}$ 0]-direction) and azimuthal (external field varied in the film plane) angular dependence of the FMR resonance field, B_{res}, measured at RT is shown in Fig. 4. The solid lines in Fig. 4 are fits according to resonance equations derived from the free energy approach discussed above (for explicit expressions of the resonance equation, see [21,22]).

Fig. 4(a) shows that for the out-of-plane geometry and for film thicknesses above 13 ML a not-aligned resonance mode was observed very close to the hard axis (similar to the case of the Fe/GaAs system). The not-aligned resonance mode is due to the collective excitation of the spin system, in which the spins precess around the equilibrium angle (depending on the internal anisotropy fields) of the magnetization instead around the external field direction. Within the geometry used for the in-plane angular dependence the not-aligned mode could be detected for the 142 ML only, most likely due to the lower sensitivity of our setup in this geometry for which the high frequency field is aligned perpendicular to the sample surface. For the out-of-plane geometry the microwave field is oriented in the film plane, yielding higher intensities due to the larger projection of the precessing magnetization vector onto the direction of the microwave magnetic field. Nevertheless, from the in-plane angular dependence a fourfold (cubic) anisotropy is observed which is superimposed by a twofold (uniaxial) contribution (see Fig. 4(b)). From the fact that *all* ⟨1 1 0⟩-directions are local maxima

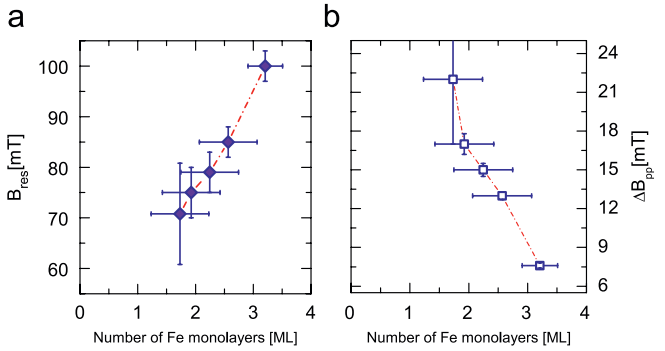

Fig. 3. Evolution of the FMR resonance field (a) and line width (b) with the equivalent number of Fe layers recorded at RT and an external magnetic field applied along the [1 $\bar{1}$ 0]-direction.

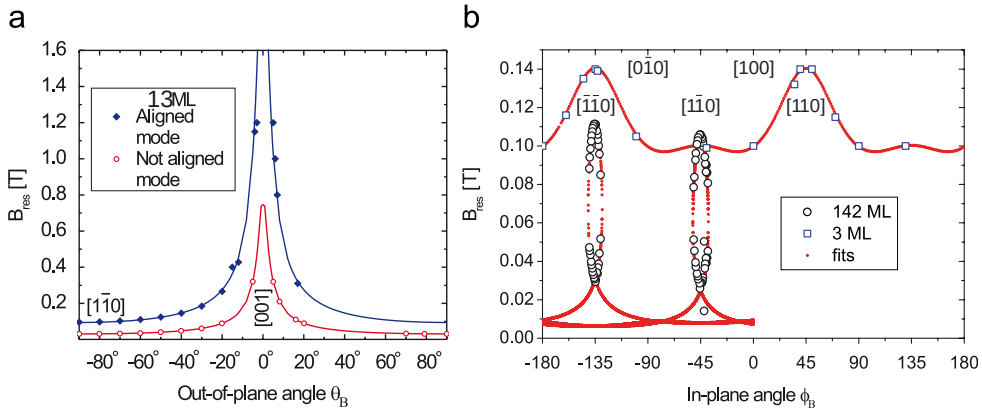

Fig. 4. Polar (a) and azimuthal (b) angular dependence of the resonance field measured at 9.3 GHz for different thick Fe layers grown on {4 × 2}InAs. The solid lines are fits to the experimental data.

Table 1
The measured magnetic anisotropy constants of uncapped Fe layers grown on {4 × 2}InAs(1 0 0) for different Fe thicknesses *d*.

d (ML)	$K_{2\perp}$ (10^6 J/m^3)	$K_{4\parallel}$ (10^4 J/m^3)	$K_{2\parallel}$ (10^4 J/m^3)	$\frac{K_{4\parallel}}{M}$ (mT)	$\frac{K_{2\parallel}}{M}$ (mT)
Bulk	–	4.8	–	27.5[a]	–
142	0.11	4.9	0.2	29.9	1.3
19	0.69	4.9	1.1	29.9	6.7
13	0.5	5.0	1.0	30.3	6.1
10	0.67	4.5	1.0	27.6	6.1
8	0.76	3.9	1.1	23.9	6.5
6	0.84	3.2	0.9	19.8	5.8
4	1.07	2.0	1.2	12.1	7.1
3	1.03	0.8	1.7	4.9	10.6

All samples were measured *in situ* at RT. The conversion to μeV/atom are given by 1×10^5 J/m^3 = 7.35 μeV/atom. The bulk value is taken from Ref. [24].

[a] Using the slightly reduced magnetization value as measured for our thin films (1640 kA/m), the bulk anisotropy field $K_{4\parallel}/M$ would take the value 29.3 mT.

one can conclude that the easy axis of the cubic anisotropy are the ⟨1 0 0⟩-directions. The easy axis of the uniaxial anisotropy is oriented along the [1 $\bar{1}$ 0]-direction as can be seen from the smaller resonance field along this direction compared to the resonance field along the [1 1 0]-direction. While for the 3 ML thick film this difference is rather obvious, for the 142 ML thick film the deviation of the resonance fields along [1 $\bar{1}$ 0]- and [1 1 0]-direction becomes less pronounced. This indicates that the ratio of cubic to uniaxial anisotropy increases with increasing film thickness. The offset of the whole angular dependence is determined mostly by the out-of-plane anisotropy that also governs the out-of-plane angular dependence shown in Fig. 4(a).

The resulting magnetic anisotropy constants from fitting the angular dependent data are listed in Table 1 for different film thicknesses (d = 3–142 ML). We additionally measured the magnetization of capped films *ex situ* with a superconducting quantum interference device (SQUID) and used $M = 1.64 \times 10^6$ A/m (which agrees with the value for Au capped films in [23]) to extract the anisotropy constants from the measured anisotropy fields ($2K_i/M$, i being the order (i.e. twofold, cubic) of the anisotropy constant).

The surface-interface, $K_i^{s,\mathrm{eff}}$, and volume, K_i^v, anisotropy contributions to the different anisotropy constants were determined by plotting the anisotropy terms vs. the reciprocal film thickness according to

$$K_i = \frac{K_i^{s,\mathrm{eff}}}{d} + K_i^v \qquad (3)$$

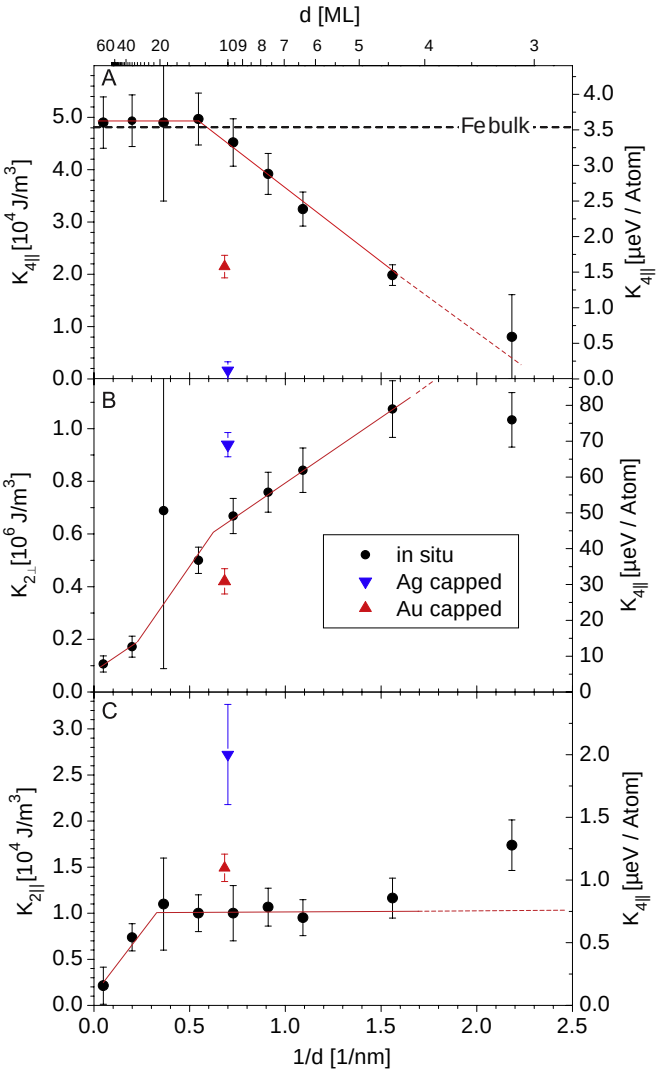

Fig. 5. Reciprocal thickness dependence of the anisotropy constants of Fe grown on {4 × 2}InAs(0 0 1). At the top the in plane cubic anisotropy constants are shown, while the uniaxial out (middle) and in plane (lowest) anisotropy are shown below that.

Fig. 5 shows the reciprocal thickness dependence of the anisotropy constants, while Table 2 summarizes the results from fitting the data points with the help of the above equation.

Table 2
Surface-interface and volume contributions to the magnetic anisotropy of uncapped Fe/{4 × 2} InAs(0 0 1) (upper part).

$K_{2\perp}^{v}$ (10^5 J/m^3)	K_{4}^{v} (10^5 J/m^3)	$K_{2\parallel}^{v}$ (10^5 J/m^3)	$K_{2\perp}^{s,\mathrm{eff}}$ (10^{-3} J/m^2)	$K_{4}^{s,\mathrm{eff}}$ (10^{-5} J/m^2)	$K_{2\parallel}^{s,\mathrm{eff}}$ (10^{-5} J/m^2)
0.7 ± 0.7	0.67 ± 0.03	0 ± 0.03	0.74 ± 0.1	-3.13 ± 0.5	3.25 ± 0.1
-2.2 ± 1.3	0.65 ± 0.03	0.025 ± 0.01	1.4 ± 0.1	-7.9 ± 0.6	—

The results of Au capped Fe/InAs measured by BLS are shown in the lower part. First line of the table: this work (investigated system vacuum/Fe/{4 × 2}InAs(0 0 1)). Second line of the table: results from Ref. [23] (investigated system Au/Fe/{4 × 2}InAs(0 0 1)).

Note that in Table 2 the first line gives our results, while the second gives the one reported in Ref. [23]. In the following the different contributions will be discussed separately.

3.2.1. Cubic in plane anisotropy $K_{4\parallel}$ (A)

The cubic anisotropy $K_{4\parallel}$ is positive for all films meaning that the favorable easy magnetization directions due to this contribution are the ⟨1 0 0⟩-directions. For thick films the cubic contribution is dominating.

It is clearly shown in Fig. 5(a), that the cubic anisotropy increases as function of film thickness until it reaches the bulk value of Fe, where it saturates at about 12 ML. All data points are located slightly above the bulk value, which at first is a surprising result. We note, however, that the anisotropy constants were calculated from the anisotropy fields by using the magnetization value obtained by SQUID for a capped film. A possible explanation could thus be that M for the uncapped films is even smaller which in term would lead to an increase of the anisotropy constants. Another source for this small deviation would be a wrong determination of the sample volume by a few percent. We also note that due to the finite size effect [25] the magnetization values for very thin films may differ from the one of the thick capped films that were used to determine M by SQUID magnetometry.

These values are different to those measured by McPhail [23]. Our films reach the bulk value at the half thickness. As one can see in Table 2, the volume contribution of this anisotropy is identical within the error bar, while the surface contribution differs in its value by a factor of 2. This most likely results from the different surfaces used (Fe/Au compared to Fe/vacuum), which influences the surface anisotropy, while it obviously has no effect on the volume contribution of the anisotropy.

3.2.2. Uniaxial out of plane anisotropy $K_{2\perp}$ (B)

The value of the perpendicular uniaxial anisotropy constant $K_{2\perp}$ in the first column of Table 1 does not dominate over the shape anisotropy given by $E_{\mathrm{Shape}} = 1/2\mu_0 M^2$ (for $M = 1.71 \times 10^6$A/m, $E_{\mathrm{Shape}} = 16.8 \times 10^5$ J/m^3). This is reflected in the value of the effective magnetization $\mu_0 M_{\mathrm{eff}} = 2K_{2\perp}/M - \mu_0 M < 0$. Consequently, the magnetization lies in the film plane for all thicknesses as can be seen from the out-of-plane angular dependence of the resonance field (see Fig. 4 (a)), where the resonance field for the in-plane direction is smallest.

Fig. 5(b) shows the uniaxial out of plane anisotropy vs. the reciprocal film thickness. As it is expected the values decreases for thicker films, but it does not fully disappear. The volume contribution is very small, but positive which does not agree with capped (which may be the origin of the difference) films discussed by McPhail.

3.2.3. Uniaxial in plane anisotropy $K_{2\parallel}$ (C)

For film thicknesses below 7 ML the in-plane uniaxial anisotropy $K_{2\parallel}$ (third column of Table 1) is the dominating in-plane term. The positive sign means that the favored easy axis is the [1 $\bar{1}$ 0]-direction. The interplay between $K_{4\parallel}$ and $K_{2\parallel}$ leads to a change of the easy axis from the [1 0 0]- toward the [1 1 0]-direction with decreasing film thickness as it will be discussed in Section 3.4.

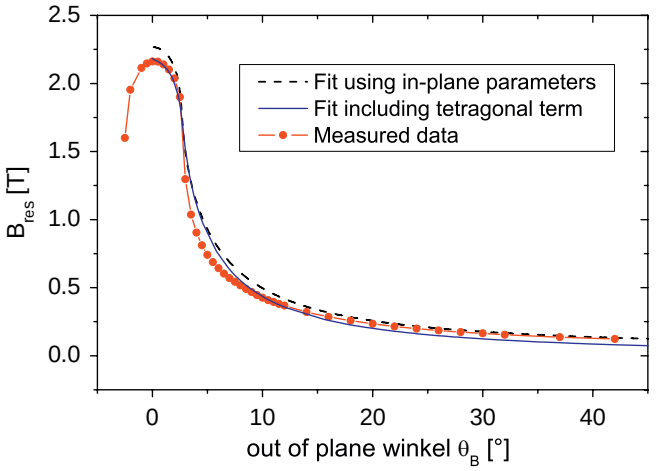

Fig. 6. Out of plane FMR measurement of 3 nm 2 nmAg/5 nm Fe/InAs(100). The 0° means that the external field is aligned perpendicular to the film plane. The fit is performed with the anisotropy values measured in plane.

There are three clearly separable regions in Fig. 5(c). For very thin films the virtual change of the uniaxial anisotropy may result from finite size effects. Thus, for films above 5 up to 20 ML the uniaxial anisotropy is nearly constant, while it starts to be reduced, although not vanishing up to 142 ML.

We propose that this stems from relaxation processes, where the islands observed in the first stage of Fe growth coalescence to a closed film at a thickness of about 20 ML, which is in accordance with our AES measurements. Indeed, at a thickness of about 20 ML difference in the growth mode is reflected by the obvious change of the $1/d$-behavior of $K_{2\parallel}$ as well as for $K_{4\parallel}$. The gradual change of $K_{2\perp}$ that does not exhibit a change at 20 ML implies that this term is mostly resulting from interface effects vanishing for thicker films.

3.2.4. Capped films

The triangles (blue and red) in Fig. 5 show clearly, that an Au or Ag cap on top of the Fe changes all anisotropy constants dramatically, which agrees with the different values measured by MacPhail. But in good agreement our Au capped film exhibits the same properties as the one reported by McPhail et al.

Even the chemical or structural difference introduced into the film surface by Au compared to Ag shows a rather large difference for $K_{4\parallel}$, $K_{2\perp}$ and $K_{2\parallel}$. This directly proves the need for *in situ* measurements in comparison to capped films. A direct comparison of the capped and uncapped films will be published later.

3.3. Out of plane measurements

In Fig. 6 an *ex situ* measurement within out of plane geometry (i.e. with the external field varying in a plane given by the film

normal and the [1 $\bar{1}$ 0]-direction) of 19 ML Fe is shown. The dashed fit curve was calculated using the values given in Table 1. The obvious deviation between fit and measurement indicates that the film does not possess perfect cubic symmetry. The deviation being largest along the film normal indicates that the film is tetragonally distorted along the film normal. This matches to the behavior within the film plane, where perfect cubic symmetry was observed and justifies the notation $K_{4\parallel}$ for the in-plane anisotropy. A tetragonal symmetry can be introduced into the resonance equation by replacing the cubic term $K_4(\alpha_x^2\alpha_y^2+\alpha_x^2\alpha_z^2+\alpha_y^2\alpha_z^2)$ within the free energy density (see Eq. (2)) by the term $-1/2K_{4\perp}\alpha_z^4-1/2K_{4\parallel}(\alpha_x^4+\alpha_y^2)$. This expression describes a tetragonal system with twofold symmetry with respect to the polar angle θ (described by the constant $K_{4\perp}$) and a fourfold one with respect to the in-plane angle ϕ (described by the constant $K_{4\parallel}$). Setting $K_{4\parallel}=K_{4\perp}:=K_4$ and using the relation $1-2(\alpha_x^2\alpha_y^2+\alpha_x^2\alpha_z^2+\alpha_y^2\alpha_z^2)=\alpha_x^4+\alpha_y^4+\alpha_z^4$ retains the expression for cubic symmetry. A detailed description of the analysis of tetragonally distorted thin films is given in [26]. The fit of the out of plane angular dependence of the 19 ML thick film yields a value of $K_{4\perp}=1.7\times10^4\,\mathrm{J/m^3}$ which is about 3 times smaller than the value for $K_{4\parallel}$ (see Table 1). We finally note that for very thin films (thickness below 10 ML), where the uniaxial anisotropy is not negligible as compared to the cubic one, the fit can be performed without tetragonal correction term.

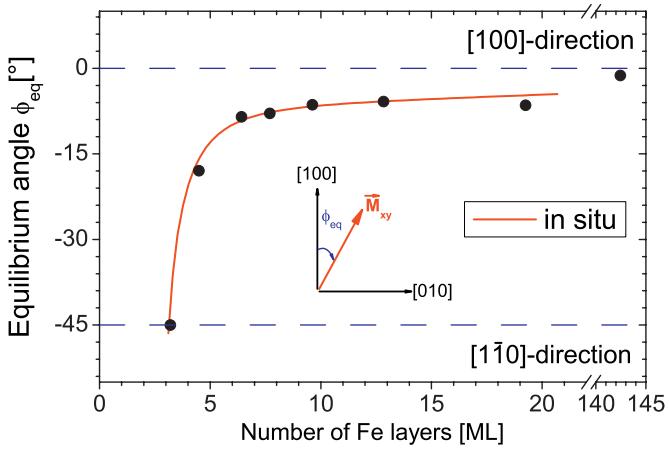

Fig. 7. The evolution of the easy axis of magnetization as a function of the number of Fe monolayers.

3.4. Thickness dependent reorientation of the easy axis

The evolution of the magnetization angle with increasing number of Fe ML was determined from the equilibrium condition, where the free energy density is minimum. The measured anisotropy constants were used to simulate the free energy density. Fig. 7 shows how the in-plane spin reorientation transition takes place. First, the easy axis is oriented along [1 $\bar{1}$ 0], rotating toward the [1 0 0]-direction for film thicknesses above 7 ML. The fact that the rotation of the easy axis occurs at smaller Fe thicknesses than for the system Fe/GaAs is related to the fact that $K_{4\parallel}$ overcomes the influence of the uniaxial in-plane anisotropy given by $K_{2\parallel}$ much faster for Fe/InAs. Even at an Fe thickness of 142 ML the magnetization is not fully aligned parallel to the [1 0 0]-direction showing that the uniaxial in-plane anisotropy still is present.

For an explanation of this not fully vanishing uniaxial anisotropy we performed Scanning Electron Microscopy (SEM), which clearly revealed island growth at the topmost part of the film. This indeed can result in an enhancement of the uniaxial anisotropy, because of stress developing at the surface of the islands, as was shown in Ref. [27]. If the islands are anisotropic stressed, an additional stress at the surface of the islands will even increase this anisotropy. An additional Ag cap layer between these islands may of course change the stress to a large extend and therefore explain our findings.

3.5. Dispersion relation

Fig. 8 shows the resonance frequency vs. resonance field (dispersion relation) for the magnetic field applied along the [1 1 0]-direction. The solid, dotted and dashed lines show the numerically calculated dispersion relation based on the resonance equation given in [21,22] for a 3, a 10 and a 19 ML sample,

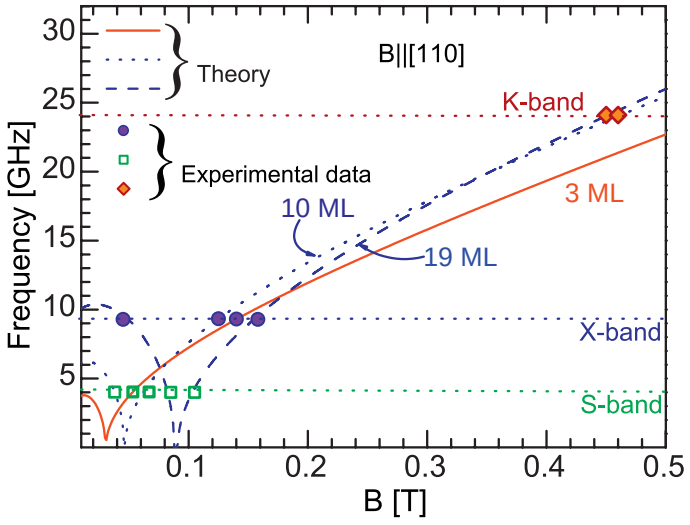

Fig. 8. Resonance frequency as a function of the resonance field for a 5, 16 and 30 ML Fe film on {4 × 2}InAs(0 0 1). The measurements were performed at RT with an external magnetic field applied along the [1 1 0]-direction.

respectively. The calculated dispersion relation predicts an not-aligned branch as was observed experimentally. At 9.3 GHz the low field (not-aligned) resonance of the 3 and 10 ML thick film cannot be excited due to the smaller cubic anisotropy. Note that the data points for $f = 24$ GHz are for 3 nm Au capped films which have been measured *ex situ* after transferring them out of the UHV system. The crossover of the curves is due to the fact that the cubic anisotropy constant is strongly thickness dependent and overcomes the uniaxial in-plane anisotropy in films with thicknesses of above 7 ML.

4. Summary

Fe ML were grown on $\{4 \times 2\}$InAs(0 0 1) by MBE. The epitaxial relationship was observed to be $[1\,0\,0]_{Fe} \| [1\,0\,0]_{InAs}$. An not closed island growing up to 19 ML was shown by our AES study. The magneto crystalline anisotropy was determined by *in situ* FMR and compared to capped ones by McPhail. The origins of the different anisotropy contributions were discussed. The volume contribution to the in-plane as well as the out-of-plane uniaxial anisotropy is proposed to be the effect of the in-plane strain and island growth. The cubic surface-interface mainly originates from the Fe surface and might be related to the reduced symmetry of the upper Fe atomic layer. The uniaxial surface term $K_{2\perp}^{s,\mathrm{eff}}$ that prefers an easy axis along the film normal, is due to the fact that the valence 3d and 4s/p electron states confined to the surface are exposed to a decreased lattice symmetry that strongly enhances the contribution of the spin–orbit interaction to the surface valence band energies, and that results in large surface magnetic anisotropies, similar to surface anisotropy in other bcc Fe films on other substrates.

Acknowledgment

This work was supported by the Deutsche Forschungsgemeinschaft, Sfb 491.

References

[1] Y.B. Xu, E.T.M. Kernohan, M. Tselepi, J.A.C. Bland, S. Holmes, Appl. Phys. Lett. 73 (3) (1998) 399–401.
[2] N. Kuze, H. Goto, M. Matsu, I. Shibasaki, H. Sakaki, J. Cryst. Growth 175–176 (2) (1997) 655.
[3] D. Grundler, Phys. Rev. Lett. 84 (26) (2000) 6074–6077.
[4] Y.B. Xu, E.T.M. Kernohan, D.J. Freeland, M. Tselepi, A. Ercole, J.A.C. Bland, J. Magn. Magn. Mater. 198–199 (1999) 703–706.
[5] H. Ohno, K. Yoh, T. Doi, A. Subagyo, K. Sueoka, K. Mukasa, J. Vac. Sci. Technol. B 19 (6) (2001) 2280–2283.
[6] L. Ruppel, G. Witte, Ch. Wöll, T. Last, S.F. Fischer, U. Kunze, Phys. Rev. B 66 (24) (2002) 245307.
[7] P. Schieffer, B. Lepine, G. Jezequel, Surf. Sci. 497 (2002) 341–348.
[8] C.M. Teodorescu, F. Chevrier, C. Richter, V. Ilakovac, O. Heckmann, L. Lechevalier, R. Brochier, R.L. Johnson, K. Hricovini, Appl. Surf. Sci 166 (2000) 124–137.
[9] M. Kneppe, M. Berse, U. Köhler, Appl. Phys. A 79 (2004) 1935–1940.
[10] C.M. Teodorescu, F. Chevriera, R. Brochierb, C. Richterb, O. Heckmannb, V. Ilakovacb, P. De Padovac, K. Hricovinib, Surf. Sci. 482–485 (2001) 1004–1009.
[11] C.M. Teodorescu, D. Luca, Surf. Sci. 600 (2006) 4200–4204.
[12] C.M. Teodorescu, F. Chevrier, R. Brochier, C. Richter, V. Ilakovac, O. Heckmann, P. De Padova, K. Hricovini, Eur. Phys. J. B 28 (2002) 305–313.
[13] M. Zwierzycki, K. Xia, P.J. Kelly, G.E.W. Bauer, I. Turek, Phys. Rev. B 67 (9) (2003) 092401.
[14] H.i Ohno, K. Yoh, K. Sueoka, K. Mukasa, A. Kawaharazuka, M.E. Ramsteiner, Jpn. J. Appl. Phys. 42 (2003) L87–L89.
[15] H. Yamaguchi, Y. Horikoshi, Phys. Rev. B 51 (15) (1995) 9836–9854.
[16] C.E.J. Mitchell Structural and electronic properties of clean (2×4) reconstructed and sulphur-pasivated InP(1 0 0), Ph.D. Thesis, Queen's University, 1996.
[17] L.E. Davis, N.C. MacDonald, P.W. Palmberg, Handbook of Auger Electron Spectroscopy, Physical Electronics Industries, Eden Prairie, 1976.
[18] Y.B. Xu, D.J. Freeland, M. Tselepi, J.A.C. Bland, Phys. Rev. B 62 (2) (2000) 1167–1170.
[19] J. Smit, H.G. Beljers, Philips Res. Rep. 10 (1955) 113.
[20] Z. Celinski, K.B. Urquhart, B. Heinrich, J. Magn. Magn. Mater. 166 (1997) 6–26.
[21] Kh. Zakeri, Th. Kebe, J. Lindner, M. Farle, J. Magn. Magn. Mater. 299 (2006) L1–L10.
[22] Kh. Zakeri, Th. Kebe, J. Lindner, C. Antoniak, M. Farle, K. Lenz, T. Tolinacuteski, K. Baberschke, Phase Transitions 79 (2006) 793–813.
[23] S. McPhail, C.M. Gürtler, F. Montaigne, Y.B. Xu, M. Tselepi, J.A.C. Bland, Phys. Rev. B 67 (2003) 0424409.
[24] C. Kittel, Introduction to Solid State Physics, Wiley, New York, 2004.
[25] R. Bergholz, U. Gradmann, J. Magn. Magn. Mater. 45 (1984) 389–398.
[26] D. Kurowski, R. Meckenstock, J. Pelzl, K. Brand, P. Sonntag, P. Grünberg, in: The 41st Annual Conference on Magnetism and Magnetic Materials, vol. 81 (8), 1997, pp. 5243–5245.
[27] S.G. Mayr, K. Samwer, Phys. Rev. Lett. 87 (3) (2001) 036105.